Strojniški vestnik - Journal of Mechanical Engineering 56(2010)10, 609-618
UDC 669.14:539.4
Paper received: 19.03.2010
Paper accepted: 15.07.2010

A Numerical and Experimental Study on Buckling of Cylindrical Panels Subjected to Compressive Axial Load

Mahmoud Shariati - Mehdi Sedighi* - Jafar Saemi - Hamid Reza Allahbakhsh
Shahroud University of Technology, Iran

In this paper, the effects of the length, sector angle and different boundary conditions on the buckling load and post buckling behavior of CK20 cylindrical panels have been investigated using experimental and numerical methods. The experimental tests have been performed using the INSTRON 8802 servo hydraulic machine and for numerical analysis. Abaqus finite element package has been used. The numerical results are in good agreement with the experimental tests.

Keywords: cylindrical panels, elastic and plastic behavior, buckling analysis, CK20 steel

0 INTRODUCTION

Shell structures have been widely used in pipelines, aerospace and marine structures, large dams, shell roofs, liquid-retaining structures and cooling towers [1]. Buckling is one of the main failure considerations when designing these structures [2]. At first, researchers focused on the determination of the buckling load in the linear elastic zone, but experimental studies [3] and [4] showed that the buckling capacity of thin cylindrical shells is much lower than the amount determined in the classic theories [5]. Thin cylindrical panels are used in different structures. When the stress distribution in this structure is compressive, the structure will collapse usually before yielding or the buckling phenomena determines its loading capacity due to the large value of radius to thickness ratio. This subject is usually studied using the numerical methods based on the finite element (FE) and analytical methods in elastic region. The exact solution for isotropic and anisotropic panels has been presented by Timoshenko [6] and Lekhnitskii [7]. El-Raheb [8] investigated the stability of simply supported panels subjected to uniform external pressure. Magnucki et al. [9] solved the Donnell's equation for the buckling of panels with three edges simply supported and one edge free subjected the axial load using the Galerkin method. Patel et al. [10] discussed on static and dynamic stability of panels with edge harmonic loading. Buermann et al. [11] presented a semi-analytical model for the post-buckling analysis of stiffened cylindrical panels using trigonometric Fourier series as approximated solutions for displacements. Lanzi et al. [12] performed a multi-objective optimization procedure based on Genetic Algorithms for the design of composite stiffened panels capable of operation in post-buckling. The results without considering any kind of imperfection, are closed and in good agreement with the tests in terms of buckling and post-buckling stiffness, as well as in terms of collapse loads. Jiang et al. [13] studied the buckling of panels subjected to compressive stress using the differential quardrature element method. Keweon [14] and [15] carried out numerical and experimental studies for the postbuckling of axially loaded cylindrical panel with curved edges clamped and with straight edges simply supported. Bisagni et al. [16] presented an analytical formulation for the study of linearized local skin buckling load and nonlinear post-buckling behavior of isotropic and composite stiffened panels subjected to axial compression. The results are compared with the FE analysis.

In this paper, numerical and experimental studies have been performed on cylindrical panels for determining the bulking load and investigating the post-bulking behavior of the panels. For a numerical analysis Abaqus FE package has been used to study the effects of the length, sector angle, thickness and different boundary conditions and the experimental tests have been applied on the panels using a servo-hydraulic machine. The experimental results are in good agreement with the experimental one.

1 PANELS GEOMETRY

Fig. 1 shows the schematic of a cylindrical panel. The mechanical properties of steel panels

*Corr. Author's Address: Shahroud University of Technology, Shahrood, I.R. IRAN, msedighi47@gmail.com

have been determined using the tensile test. The steel grade is CK20. For this purpose, some standard test specimens have been prepared from the original tubes according to ASTM E8 standard [10] and the tensile test was performed using the INSTRON 8802 tensile test machine. Fig. 2 shows the stress-strain diagram for the material of a specimen. The Poisson's ratio was assumed to be 0.33. The geometrical and mechanical properties of panels have been listed in Table 1.

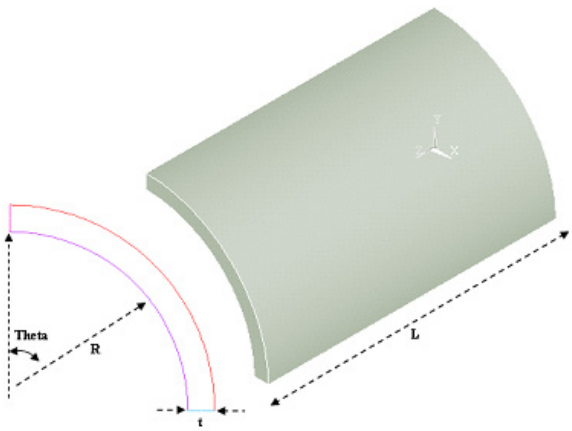

Fig. 1. *Schematic of a cylindrical panel*

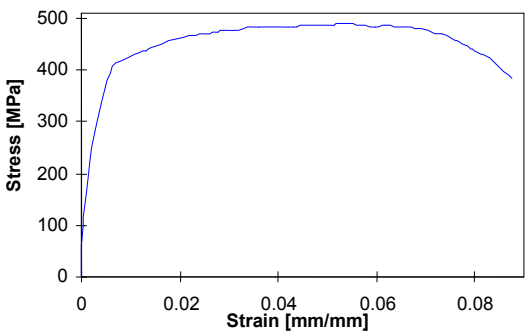

Fig. 2. *Stress-strain diagram*

Table 1. *Mechanical and geometrical properties of cylindrical panels*

Diameter	$D = 42$ mm
Thickness	$T = 2$ mm
Sector angle	$\Theta = 90°, 120°, 180°, 355°,$ Complete
Length	$L = 100, 150, 250$ mm
Yield stress	$\sigma_y = 340$ [MPa]
Elasticity modulus	$E = 192$ [GPa]

2 BOUNDARY CONDITIONS

For applying boundary conditions on the edges of the cylindrical panel, two rigid plates that were attached to the ends of the cylindrical panel were used. In order to analyze the buckling subject to axial load similar to what was done in the experiments; a 15 mm displacement was applied centrally to the center of the upper plate, which resulted in a distributed, compressive load on both edges of the cylindrical panel. Additionally, all degrees of freedom in the lower plate and all degrees of freedom in the upper plate, except in the direction of longitudinal axis, were constrained. In the section on experimental results, it will be shown that the fulcrum used in these tests has an edge that is 18.1 mm high (Fig. 3). For this reason, in numerical simulations, the edges of the shell are constrained to this elevation except in the direction of cylinder axis.

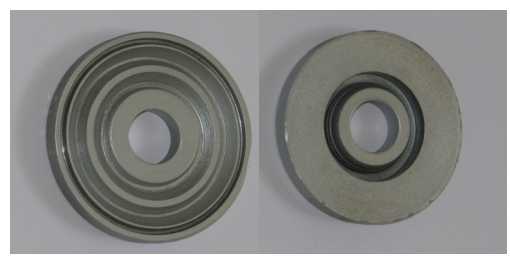

a **b**

Fig. 3. *Fixtures for experimental test: a) simply support, b) clamped*

3 NUMERICAL ANALYSIS

The numerical analysis has been performed with Abaqus FE package. For this analysis, the nonlinear element S8R5, which is an eight-node element with six degrees of freedom per node, suitable for analysis of thin shells, and the linear element S4R, which is a four-node element were used [18]. Part of a meshed specimen is shown in Fig. 4. Both linear and nonlinear elements were used for the analysis of the shells, and the results were compared.

The boundary conditions have been considered clamped or simple at arc edges and free at straight edges. Eigenvalue analysis overestimates the value of buckling load, because in this analysis the plastic properties of a material do not play any role in the analyses procedure. For buckling analysis, an eigenvalue analysis

should be done initially for all specimens to find the mode shapes and corresponding eigenvalues. Primary modes have smaller eigenvalues and buckling usually occurs in these mode shapes. For the eigenvalues analysis the ‘‘Buckle’’ step was used in software. Three initial mode shapes and corresponding displacements of all specimens were obtained. The effects of these mode shapes must be considered in nonlinear buckling analysis (Static Riks step). Otherwise, the software would choose the buckling mode in an arbitrary manner, resulting in unrealistic results in nonlinear analyses. For ‘‘Buckle’’ step, the subspace solver method of the software was used. It is noteworthy that due to the presence of contact constraints between rigid plates and the shell, the Lanczos solver method cannot be used for these specimens [18]. In Fig. 5, two primary mode shapes are shown for the specimen L100-θ90°. After completion of the Buckle analysis, a nonlinear analysis was performed to plot the load–displacement curve. The maximum value in this curve is the buckling load.

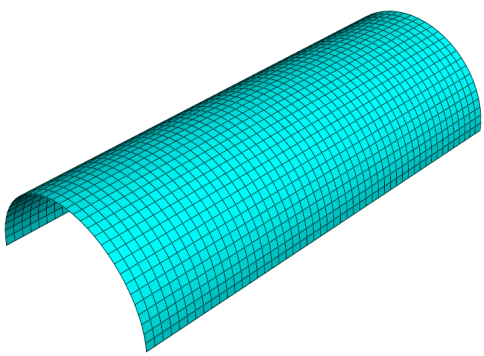

Fig. 4. *Mesh pattern for a cylindrical panel*

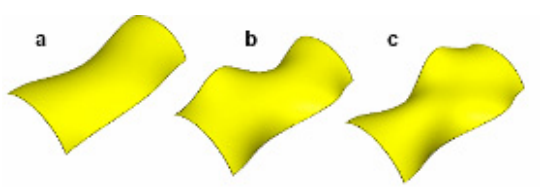

Fig. 5. *Buckling mode shape for specimen L = 100 mm, θ = 90°: a) first mode, b) second mode, c) third mode*

This step is called ‘‘Static Riks’’ and uses the arc length method for post-buckling analysis. In this analysis, nonlinearity of both material properties and geometry is taken into consideration.

4 EXPERIMENTAL ANALYSIS

Some specimens with characteristics listed in Table 1 were prepared and the compression test was applied using a servo-hydraulic machine on panels. At first, for investigating the reliability of system for repeating the tests, three similar panels with $L = 100$ mm and , $\theta = 120^{\circ}$ were tested. Fig. 6 shows the load–displacement diagrams for these panels. It is clear that the results are the same and the machine is reliable so the tests can be repeated.

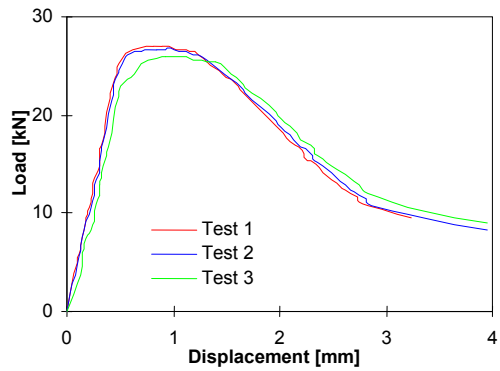

Fig. 6. *Load-displacement diagrams for three similar panels with L = 100 mm, θ = 120°*

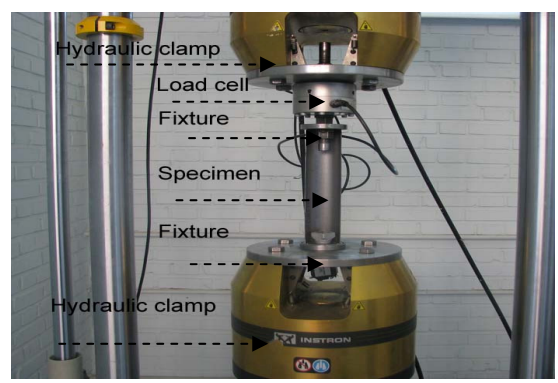

Fig. 7. *Experimental test setup*

For different boundary conditions, the axial load was applied on the panels and the load-axial displacement diagrams of panels were drawn. In all the tests, the straight edges were free and the arc edges were clamped or simply supported. To produce the clamped and simple boundary conditions, some appropriated fixtures were designed. Fig. 7 shows the test setup.

5 DISCUSSION OF RESULTS

Fig. 8 shows the numerical and experimental load-displacement diagrams for panels with different lengths. The peak values in diagrams stand for the buckling load. Figs. 9 and 10 show the load-displacement diagrams for $\theta = 90°, 180°$.

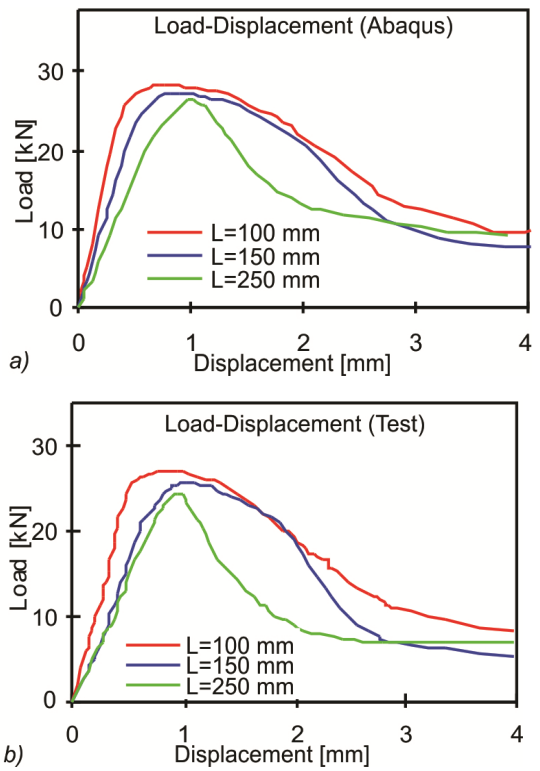

Fig. 8. *Load-displacement diagrams for different lengths ($\theta = 120°$, simply supported): a) numerical analysis, b) experimental test*

It can be seen that by increasing the length of the panel, the buckling load slightly decreases. These variations are more for shorter lengths. For longer lengths, the load-displacement diagram for the smallest sector angle i.e. $\theta = 90°$ (Fig. 9) tends to Euler's buckling mode. Fig. 11 shows that by increasing the sector angle, the buckling load increases. When there is a narrow cut ($\theta = 355°$), the buckling load decreases noticeably. The variations of the buckling load in terms of the sector angle are shown in Fig. 12. Its variation is nearly linear and it changes very large for a cylinder. Fig. 13 shows the deformed shape of a panel with a narrow cut.

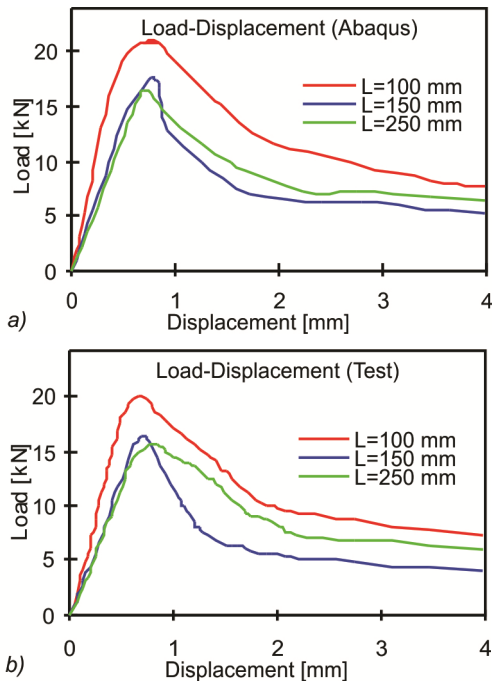

Fig. 9. *Load-displacement diagrams for different lengths ($\theta = 90°$, simply supported): a) numerical analysis, b) experimental test*

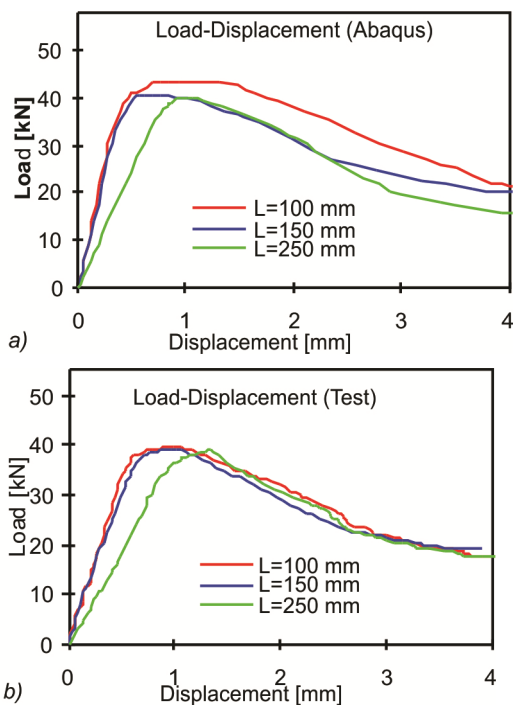

Fig. 10. *Load-displacement diagram for different lengths ($\theta = 180°$, simply supported): a) numerical analysis, b) experimental test*

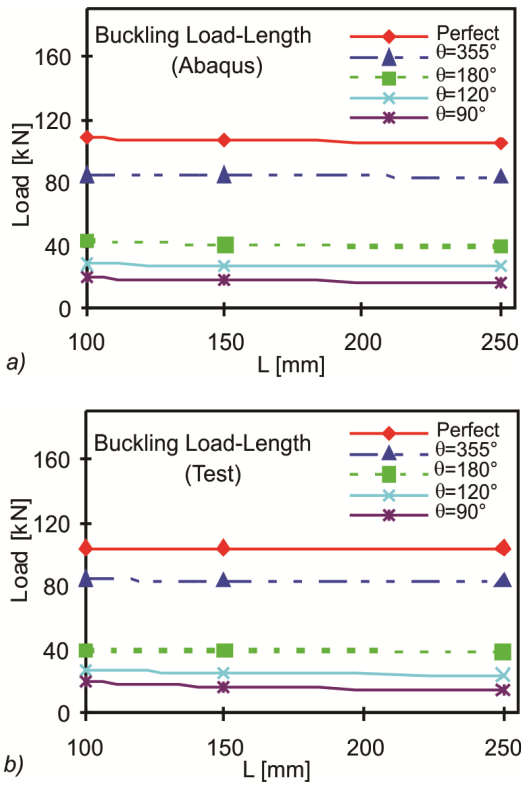

Fig. 11. *Buckling load in terms of the length for different sector angles: a) numerical analysis, b) experimental test*

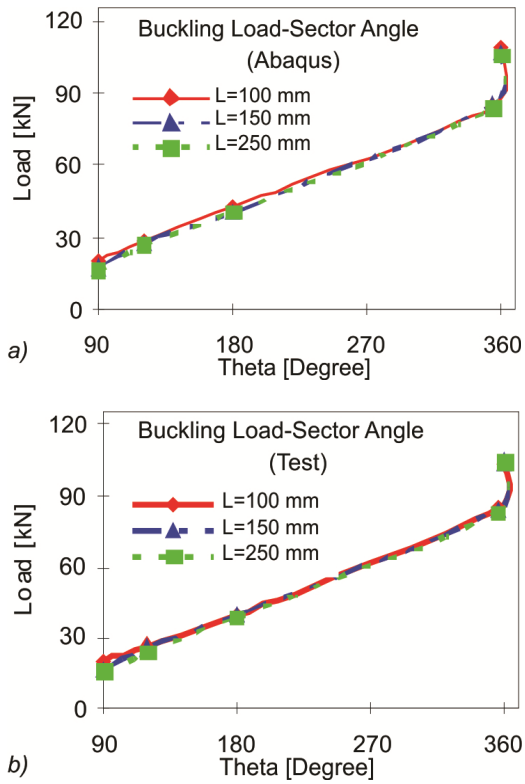

Fig. 12. *Buckling load in terms of the sector angle for different lengths (simply supported): a) numerical analysis, b) experimental test*

The load-displacement diagrams and the first buckling modes for different panels are shown in Table 2. The buckling modes are similar and there is a good agreement between the load-displacement diagrams in most cases.

Most differences between the diagrams return to the post buckling region and the values for FE results are greater than the test values. This may be due to the approximated definition of the plastic part of the stress-strain diagram and no consideration of the specimens defects in FE model. The FE stress analysis shows that in some cases, the Von-Mises stresses in panels are larger than the yield stress or the panel is not elastic at the buckling load. Fig. 14 shows the Von-Mises stresses of a panel under buckling load.

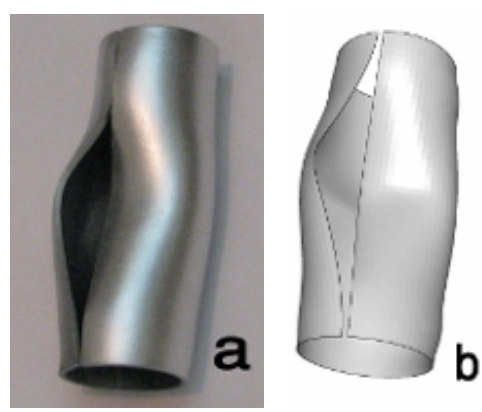

Fig. 13. *Deformed shaped of panel (θ = 355°, L = 150 mm, simply supported): a) experimental, b) numerical*

Table 2. *Numerical and experimental load-displacement diagrams and buckling modes for different lengths and sector angles*

Numerical mode	Experimental mode	Load–displacement diagrams
		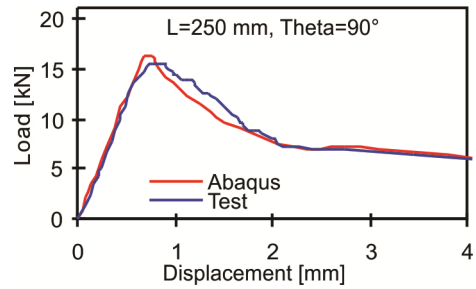
		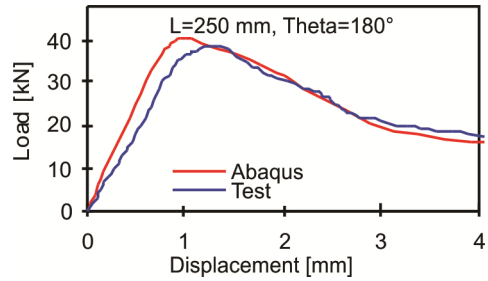
		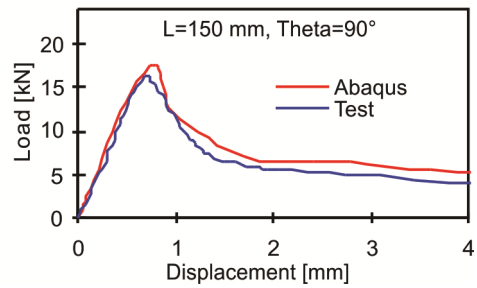
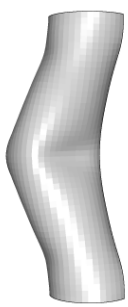		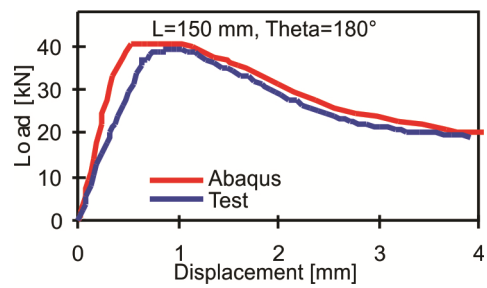

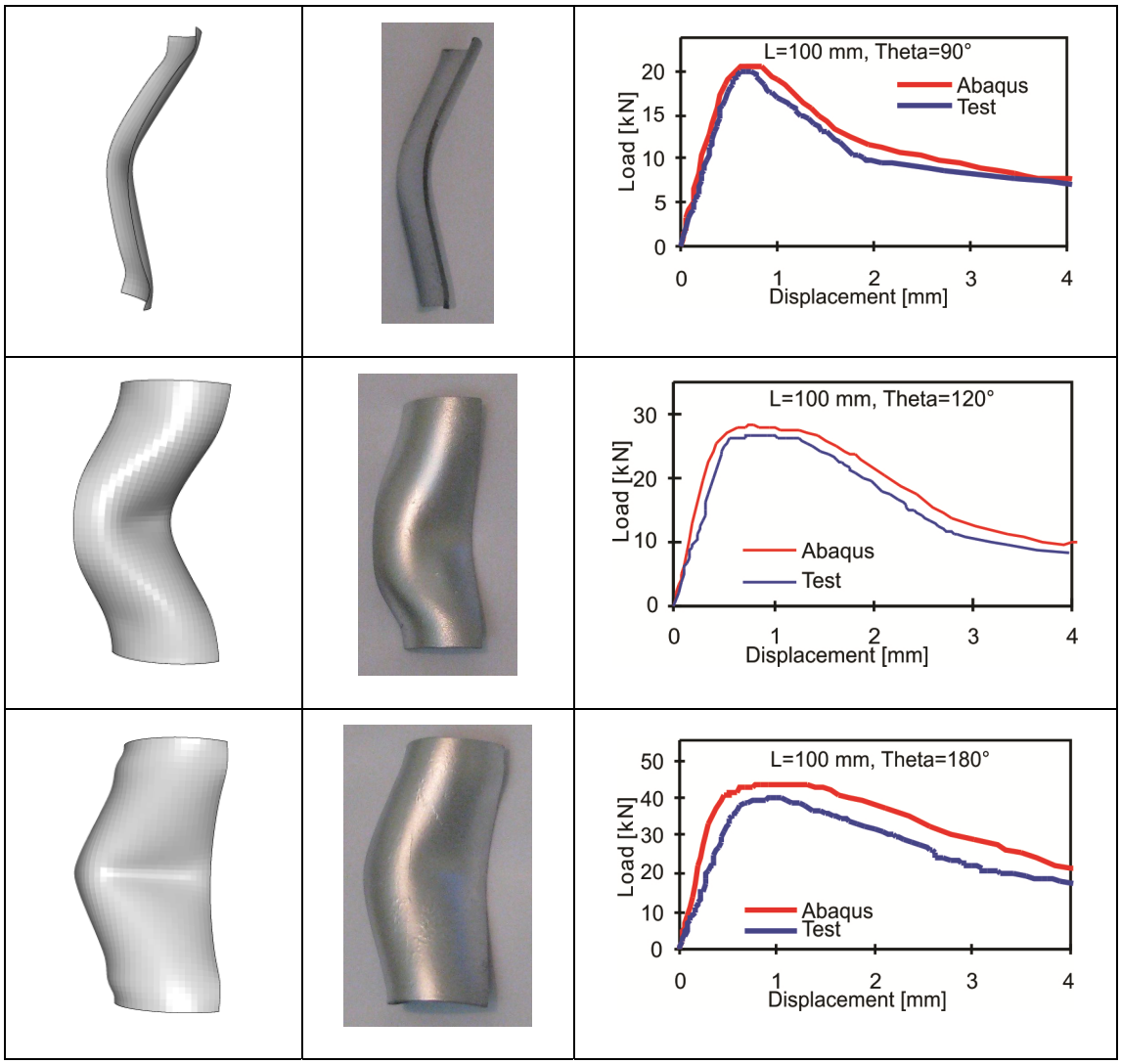

6 EFFECTS OF BOUNDARY CONDITIONS

To investigate the effects of different boundary conditions, some tests were performed on the panels with clamped and simple supports. Table 3 shows the load-displacement diagrams for clamped and simply supported boundary conditions. The results show that in all tests, the clamped boundary conditions can increase the buckling load capacity of the panels. This is because the clamped boundaries can restrict the degrees-of-freedom. The Euler buckling mode has been seen for L = 250 mm and θ = 120° in numerical and experimental results. The values of buckling loads for these boundary conditions are listed in Table 4.

After comparing the curves in Fig. 15, it can be said that in comparison to nonlinear elements, linear elements, have a better prediction power for the post-buckling behavior of mild steel alloy cylindrical shells with elliptical cutouts. In the prebuckling phase, both elements produce similar results.

It can be seen that the slope of load vs. end shortening curves is higher in numerical results than in experimental results before the buckling. This discrepancy is the result of the presence of internal defects in the material which reduces the stiffness of the specimens in the experimental method, while the materials are assumed to be ideal in the numerical analyses.

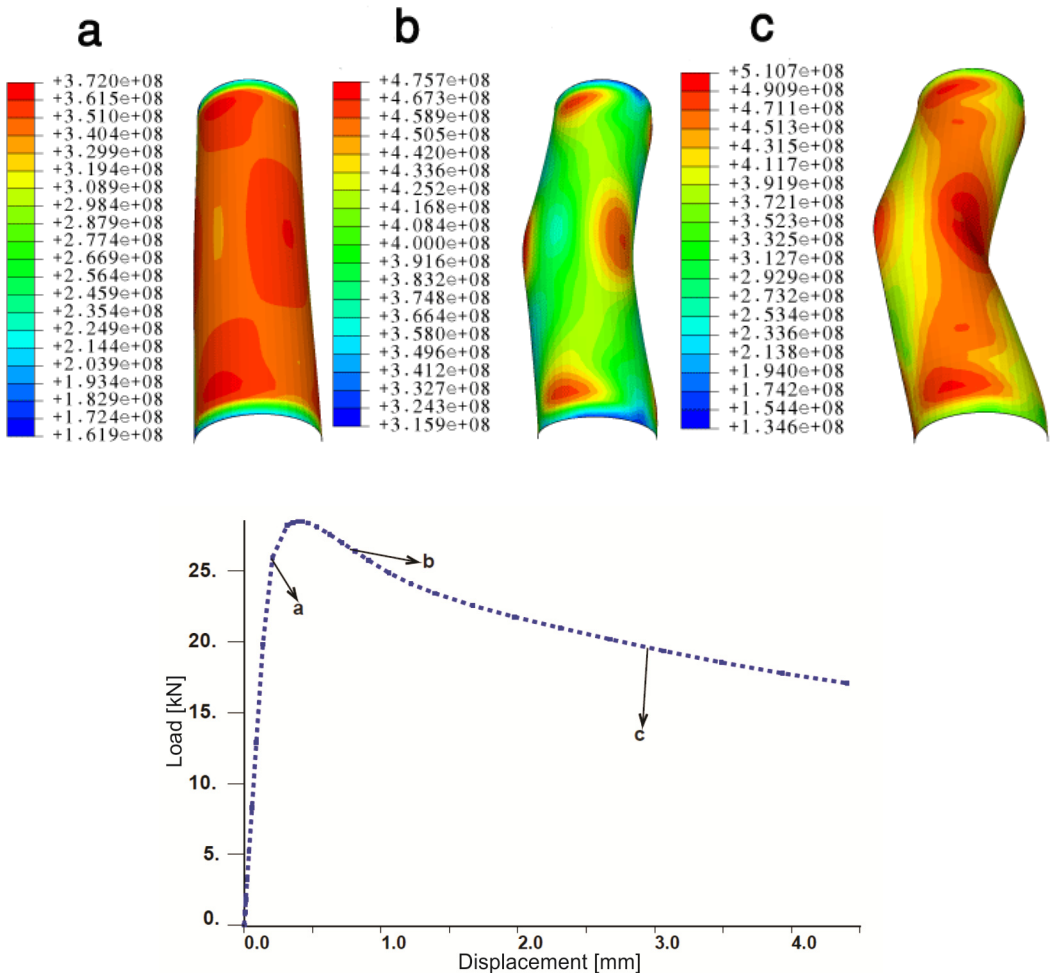

Fig. 14. *Von-Mises stress (Pa) distribution in panel due to different loads (simply supported): a) applied load is in elastic region, b and c) applied loads are in post-buckling region*

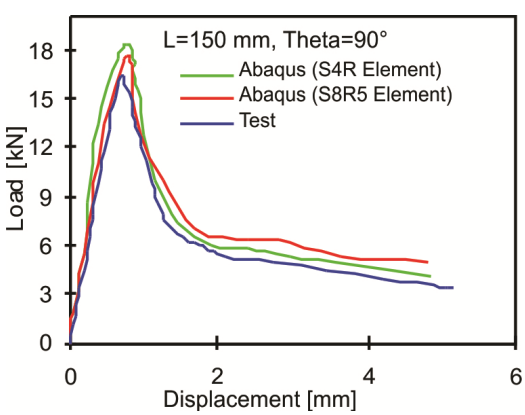

Fig. 15. *Comparison of the experimental and numerical result*

7 CONCLUSIONS

The experimental tests and numerical analysis which were performed on the panels showed that:

1. Increasing the length will slightly decrease the buckling load. This effect is more important for shorter panels.
2. By increasing the sector angle, the buckling load will increase nearly linearly and for a perfect cylinder, it changes more.
3. The existence of a longitudinal narrow slot will decrease the buckling load noticeably.
4. The clamped boundary conditions will increase the capacity of the panel to undergo the load or the buckling load will increase.

5. In most of the analysis, there are good agreements between the numerical and experimental results.
6. The results show that the curves from linear elements predict the post-buckling region better than nonlinear elements, while the nonlinear elements are a better indicator of the buckling load.

Table 3. *Load-displacement diagrams for clamped and simply supported boundary conditions*

Numerical	**Experimental**
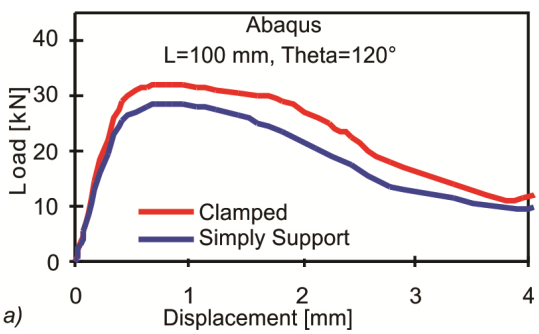	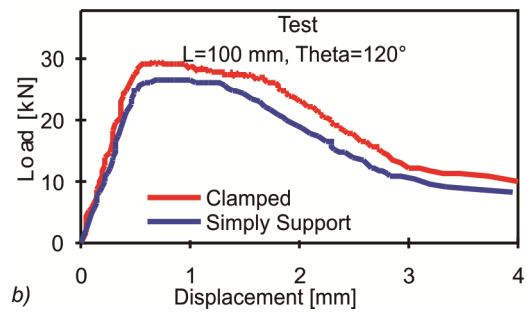
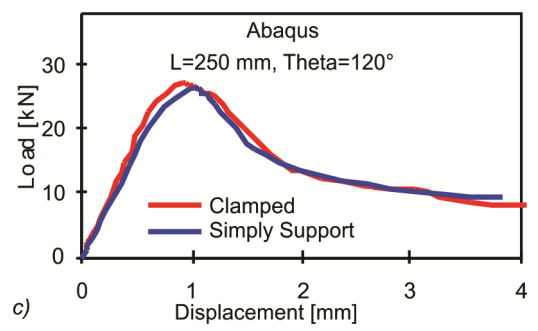	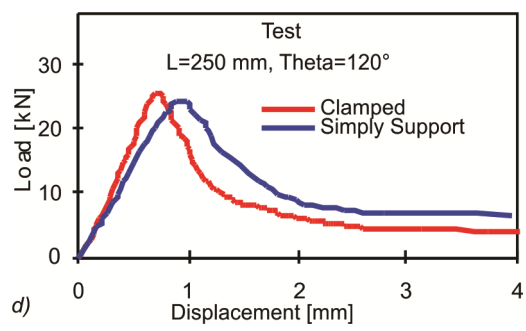

Table 4. *Buckling load [kN] for different boundary conditions*

θ = 120 °	L = 100 mm		L = 150 mm		L = 250 mm	
	Numerical	Experimental	Numerical	Experimental	Numerical	Experimental
simply supported	28.23	26.75	27.29	25.55	26.37	24.34
clamped	32.02	29.56	30.76	26.04	27.21	25.58

8 ACKNOWLEDGEMENT

The authors thank the Manager of the "Mechanical Properties Laboratory" of Shahrood University of Technology for supporting the tests.

9 REFERENCES

[1] Farshad, M. (1992). *Design and analysis of shell structures*, Kluwer, Dordrecht.

[2] Budiansky, B., Hutchinson, J.W. (1972). Buckling of circular cylindrical shells under axial compression. *Contributions to the*

theory of aircraft structures. Delft University Press, p. 239-260.

[3] Arbocz, J., Hol, J.M.A.M. (1991). Collapse of axially compressed cylindrical shells with random imperfections. *AIAA J.,* vol. 29, p. 2247-2256.

[4] Jullien, J.F., Limam, A. (1998). Effect of openings on the buckling of cylindrical shells subjected to axial compression. *Thin Wall Struct*, vol. 31, p. 187-202.

[5] Farshad, M. (1994). *Stability of structures*. Elsevier, Amsterdam.

[6] Timoshenko, S.P., Gere, J.M. (1961). *Theory of elastic stability*. McGraw-Hill, NewYork.

[7] Lekhnitskii, S.G. (1968). *Anisotropic plates*. Gordon and Breach, NewYork.

[8] El-Raheb, M. (2006). Response of a thin cylindrical panel with constrained edges. *Int J. Solids Structures,* vol. 43, p. 7571-7592.

[9] Magnucki, K., Mackiewicz, M. (2006). Elastic buckling of an axially compressed cylindrical panel with three edges simply supported and one edge free. *Thin-Walled Structures,* vol. 44, p. 387-392.

[10] Patel, S.N., Datta, P.K., Sheikh, A.H. (2006). Buckling and dynamic instability analysis of stiffened shell panels. *Thin-Walled Structustures*, vol. 44, p. 321-333.

[11] Buermann, P., Rolfes, R., Tessmer, J., Schagerl, M. (2006). A semi-analytical model for local post-buckling analysis of stringer- and frame-stiffened cylindrical panels. *Thin-Walled Structures*, vol. 44, p. 102-114.

[12] Lanzi, L., Giavotto, V. (2006). Post-buckling optimization of composite stiffened panels: Computations and experiments. *Composite Structures*, vol. 73, no. 2, p. 208-220.

[13] Jiang, L., Wang, Y., Wang, X. (2008). Buckling analysis of stiffened circular cylindrical panels using differential quadrature element method. *Thin-Walled Structures,* vol. 46, p. 390-398.

[14] Bisagni, C., Vescovini, R. (2009). Analytical formulation for local buckling and post-buckling analysis of stiffened laminated panels. *Thin-Walled Structures*, vol. 47, p. 318-334.

[15] Kweon, J.H., Hong, C.S. (1994). An improved arc-length method for postbuckling analysis of composite cylindrical panels. *Computers Structs*, vol. 53, no. 3, p. 541-549.

[16] Kweon, J.H. (1998). Post-failure analysis of composite cylindrical panels under compression. *J. Reinforced Plastics Composites*, vol. 17, no. 18, p. 1665-1681.

[17] ASTM A370-05, *Standard test methods and definitions for mechanical testing of steel products.*

[18] *ABAQUS 6.4 PR11* user's manual.